Design and Simulation of an Improved Energy Selective Surface

Bo Yi*, **Yanfei Dong, Cheng Yang, Peiguo Liu, and Yan Li**

Abstract—Energy selective surface (ESS) proposed in recent years is one of the most effective means for defending high intensity electromagnetic wave attacking. This paper presents an improved ESS structure and its systematic design method. An ESS prototype is designed and fabricated based on a given requirement. Its insertion loss is measured in an anechoic chamber, and its shielding effectiveness is tested under HPM and UWB irradiation. Measured results show that the ESS sample meets the given requirement.

1. INTRODUCTION

During past decades, high power electromagnetic sources and wideband technologies have achieved notable progress and electromagnetic weapons become assessable to offenders [1, 2]. Electromagnetic weapons can be as small as a suitcase and carried into a building with public access [3]. They can irradiate high intensity electromagnetic wave: high power microwave (HPM) and ultra-wideband source (UWB), both with an intensity about $10\,\text{kV/m}$ at target place (dependence on range) and pose a serious threaten to most information equipments [4]. The most effective way to protect information equipments is to put them in shielding room [5]. But this method cannot be applied to facilities needed to interact with outer environment. Aiming at protecting these facilities, many protection methods, like carbon foam, manganite films and frequency selective surface (FSS), are proposed [6, 7]. Usually, high intensity electromagnetic wave may couple in electronic and electrical systems through "Front door" such as antennas and "back door" such as cables, apertures [8, 9]. Among them, antenna provides an important channel for high intensity electromagnetic wave entering information systems. FSS as a protecting method has been studied for many decades [10]. But it will fail to provide protection when the frequency of high intensity electromagnetic wave is located within its passband. In order to overcome this defect, limiting FSS was designed in [11, 12]. It can change its passband when high intensity electromagnetic wave arrives. Scott et al. adopted FSS loaded phase change material to realize adaptive protection [13]. At a given temperature, the resistivity of phase change material decreases abruptly, typically by three orders of magnitude. But some time is needed for temperature of phase change material increasing and reaching the threshold; therefore, some part of the energy may leak into receiver front end. Plasma limiter is another method of adaptive protection against high electromagnetic waves [14].

The concept of energy selective surface (ESS) as a new self-actuated protection method has been proposed in [5]. Compared with the adaptive protection methods mentioned above, ESS pays more attention to amplitude of incident wave instead of frequency. In other words, ESS can realize ultra wideband defending. Using proper diodes as the switchable device, the response time of ESS only needs several nanoseconds under UWB irradiation and within $100\,\text{ns}$ under HPM irradiation.

The ESS structure in [5] validates the concept of energy selection. This paper improves the structure of ESS and presents systematic design method for it as well. Compared with the energy selective

structure in [5], the improved ESS expands the working band. In Section 2, the equivalent circuit theory about metallic strip is introduced. Simulations for ESS are conducted in Section 3. In Section 4, the experiments are carried out in anechoic chamber for insertion loss and in open environment for shielding effectiveness under HPW and UWB irradiation. In Section 5, conclusions are drawn.

2. ANALYSIS AND SIMULATION OF IMPROVED ESS UNIT CELL

In this section, energy selective mechanism is firstly introduced. This mechanism implies that ESS is transparent to low intensity electromagnetic wave while shielding high intensity one in working band [7]. In order to realize energy selective mechanism, ESS needs a variable impedance surface. PIN diode is one of the good choices as a nonlinear device mounted on the metal unit cell to achieve variable impedance surface. A conductor cross patch usually has a higher resonant frequency than a loop patch with same period [15]. So the conductor cross patch is more suitable for constructing ESS. The property of diode loaded conductor cross patch with arbitrary polarization direction can be estimated by studying the rectangle patch with diode loaded only valid for an incident wave at a specific polarization direction [16]. So the unit cell of ESS can be simplified to the structure shown in Figure 1. Here, D and W represent the length and width of ESS unit cell, respectively. w_0 denotes the width of metallic patch. d_0 and d_1 represent the length of metallic patch and width of slot between adjacent metallic patches, respectively. Figure 1 also presents equivalent metal structure of ESS unit cell when diode is on and off.
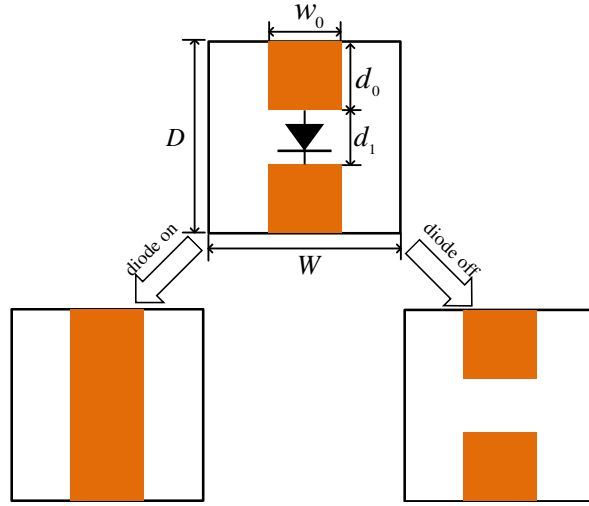

Figure 1. The unit cell of ESS and its equivalent circuit when diode on or off.

The equivalent circuits of ESS unit cell in Figure 1 are shown in Figure 2. PIN diode is replaced by its reverse and forward bias equivalent circuit model, and metal patch is replaced by inductor [17]. The slot between adjacent metallic patches is equivalent to a capacitor.

In Figure 2, C_1 and L_1 represent the equivalent capacitance and inductance of metallic strips, respectively. Z_0 and L_2 denote the characteristic impedance of space and package inductance of PIN diode, respectively. In Figure 2(a), R_f represents the equivalent forward resistance when PIN diode is on. In Figure 2(b), C_2 and R_r denote the equivalent package capacitance and reverse resistance, respectively, when PIN diode is off. L_2, R_f, C_2 and R_r can be estimated based on the measured S parameters.

When the electric field polarization is parallel to the metallic edges, the metallic strips are inductive and can be replaced by inductor. We can also estimate the equivalent inductance L per unit length as follows [18].

$$L = \frac{\mu_0 d}{2\pi} \left(\ln \csc \left(\frac{\pi w}{2W} \right) + G_x \right) \tag{1}$$
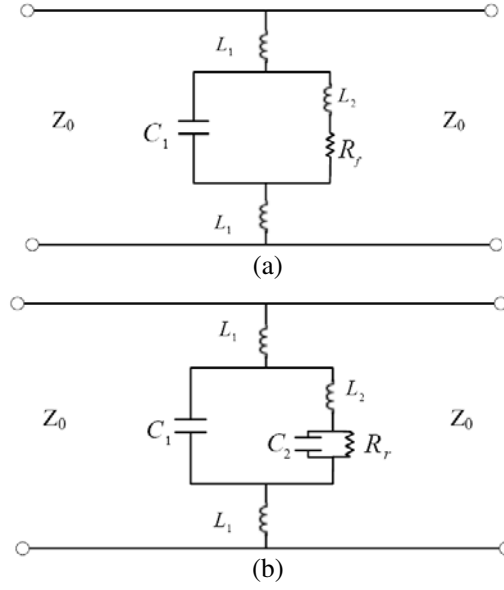
Figure 2. Equivalent circuit of ESS unit cell. (a) Equivalent circuit of ESS when PIN diode is on. (b) Equivalent circuit of ESS when PIN diode is off.

$$G_x = \frac{1}{2} \frac{(1 - \beta_x^2)^2 \left(2A_x \left(1 - \frac{\beta_x^2}{4}\right) + 4A_x^2 \beta_x^2\right)}{1 - \frac{\beta_x^2}{4} + 2A_x\beta_x^2 \left(1 + \frac{\beta_x^2}{2} - \frac{\beta_x^4}{8}\right) + 2A_x^2\beta_x^6} \tag{2}$$

$$A_x = \frac{1}{\sqrt{1 - \left(\frac{W}{\lambda}\right)^2}} - 1 \tag{3}$$

$$\beta_x = \sin\frac{\pi w}{2W} \tag{4}$$

where, w and W denote the width of metal strip and unit cell, respectively.

When the electric field polarization is perpendicular to the metallic edges, the metallic strips are capacitive and can be replaced as capacitor. We can also estimate the equivalent capacitance C per unit width as follows.

$$C = \frac{2\xi_0 wD}{\pi W} \left(\ln \csc\left(\frac{\pi d}{2D}\right) + G_b\right) \tag{5}$$

$$G_b = \frac{1}{2} \frac{(1 - \beta_b^2)^2 \left(2A_b \left(1 - \frac{\beta_b^2}{4}\right) + 4A_b^2 \beta_b^2\right)}{1 - \frac{\beta_b^2}{4} + 2A_b\beta_b^2 \left(1 + \frac{\beta_b^2}{2} - \frac{\beta_b^4}{8}\right) + 2A_b^2\beta_b^6} \tag{6}$$

$$A_b = \frac{1}{\sqrt{1 - \left(\frac{D}{\lambda}\right)^2}} - 1 \tag{7}$$

$$\beta_b = \sin\frac{\pi d}{2D} \tag{8}$$

where d is the width of metallic strips edges.

The thin substrate also has an impact on the equivalent capacitance. But its influence is small and often ignored.

The ESS transmission coefficient T can be calculated as follows:

$$T = \frac{2Z_{\text{ESS}}}{2Z_{\text{ESS}} + Z_0} \tag{9}$$

where, Z_{ESS} represents the surface impedance of ESS.

3. SIMULATION AND DESIGN OF IMPROVED ESS

3.1. Structural Parameters Analysis

In order to design a proper ESS, we first study the influence of each structural parameter to its performance through simulation in CST MWS.

Select the parameters in Table 1 to construct ESS and keep them unchange unless special declaring. Rogers RO4350 was chosen as substrate material, and its thickness was set to 0.5 mm. In simulation, diode was replaced by capacitor and inductor in series at zero bias and by resistor and inductor in series at forward bias. Some useful results can be obtained by undertaking simulation with different conditions [7]. In order to decrease starting threshold, PIN was mounted on the place where electric field was maximal.

Table 1. Geometrical parameters list for ESS.

Parameter	Dimensions (mm)
W	6
D	6
w_0	5.5
d_0	2.6
d_1	0.8

Table 2 summarized the relationship between structural size and transmission characteristic based on simulation and calculation results based on the equivalent circuit.

Table 2. The relationship between structural size and transmission characteristic.

Parameter	Insertion loss	Shielding effectiveness
W/D	↓↓	↓↓
$W(W/D = \text{constant})$	↓↓	↑↑
w_0/W	↑	↑
d_1/D	↓	↓

In Table 2, symbols ↑↑ and ↑ represent that the parameter is positively related to the performance of ESS. Symbols ↓↓ and ↓ represent that the parameter is negatively related to the performance. ↑↑ and ↓↓ indicate that the parameter has great impact on ESS performance. ↑ and ↓ indicate that the parameter has moderate impact on ESS performance.

The conclusions drawn in Table 2 were helpful for designing improved ESS. From Table 2, we know that the size of period has great influence on both insertion loss and shielding effectiveness. In the process of designing ESS, the size of period should be decided both by requirement of insertion loss and shielding effectiveness and by starting threshold. From the second row of Table 2, we know that smaller size of period corresponds to better performance of ESS. But too small a size may lead to starting threshold increasing. In order to meet the requirement of insertion loss and shielding effectiveness at same time, width W of period should be set the same as length D of period. In general, the width of metal patch is as wide as possible for gaining higher shielding effectiveness. But too wide a patch may lead to high insertion loss.

In order to reduce insertion loss, rectangular patch can be replaced by the patch shown in Figure 3. The improved patches increase the gap between adjacent patches and reduce the equivalent capacitance of metal patches essentially. In other words, the ESS based on improved shape has a lower insertion loss than the ESS based on rectangular shape.
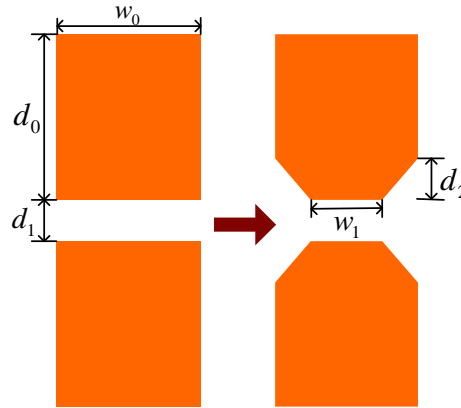
Figure 3. Improved metal patch shape.

Figure 4 shows the comparison of transmission performance between ESS and improved ESS. As shown in Figure 4(a), the improved ESS has a lower insertion loss than the ESS. Meanwhile, the shielding effectiveness of improved ESS almost keeps the same.
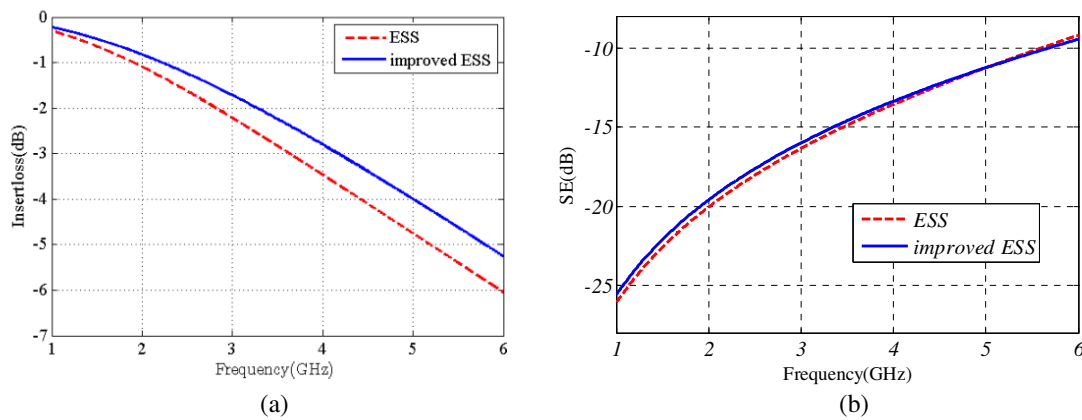
Figure 4. Comparison of transmission performance between ESS and improved ESS. (a) Comparison of insertion loss between ESS and improved ESS. (b) Comparison of shielding effectiveness between ESS and improved ESS.

3.2. Example of Designing Improved ESS

Based on the conclusions above, an ESS was fabricated, and the requirement of it is shown in Table 3.

Table 3. The given protection requirement of ESS.

defending frequency	Insertion loss	Shielding effectiveness	Starting threshold
$< 1.5\,\text{GHz}$	$< 1\,\text{dB}$	$> 15\,\text{dB}$	$< 1000\,\text{V/m}$

In order to meet the requirement of a low insertion loss and a proper shielding performance at same time, the size of period should be smaller than $\lambda/30$ empirically, where λ is the wavelength of the highest working frequency. In this case, the highest frequency is 1.5 GHz. For PIN diodes, 0.7 V is enough to turn it on and become a conductor in DC. But the forward voltage of PIN diode will increase when working in radio frequency. We chose bap6302 as the loaded diode. Its equivalent capacitance is about 0.12 pf, and its equivalent resistance and inductance are about $1.74\,\Omega$ and 0.75 nH, respectively calculated based on measured S parameters at L band. According to measured results, the turn-on voltage of bap6302 PIN diode is about 5 V at 1.5 GHz. So the period size should be bigger than 5 mm. Based on the consideration above, the size of period was set to 6 mm. The value of parameters in Table 1 can be used to construct the ESS based on the above discussion. Considering the size of PIN diode and convenience to solder it, w_1 was set to 0.8 mm and d_2 set to 0.5 mm.

In order to study the influence of ESS on antenna pattern, a horn loaded with an improved ESS at its aperture was simulated in CST MWS. Figure 5 shows the comparison of the field patterns of horn antenna directional diagram between mounted and unmounted ESS. We find that ESS only slightly changes the side lobe of the horn antenna and has little influence on its main lobe at both E and H planes.
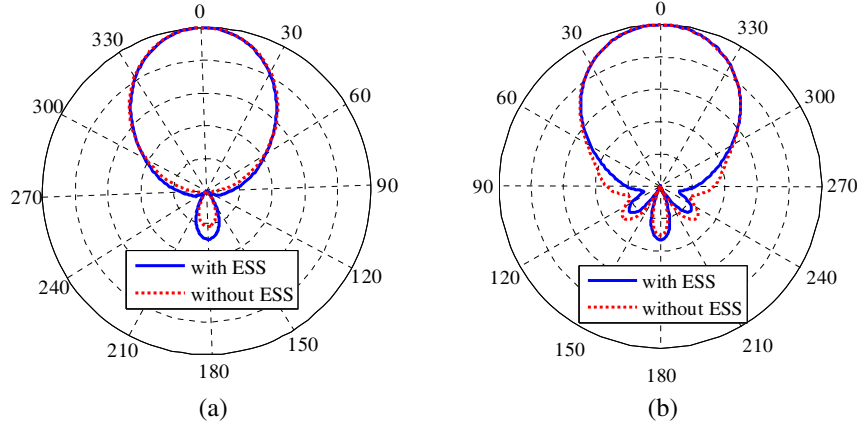
Figure 5. The compare between horn antenna's directional diagram with and without ESS. (a) H-plane directional diagram. (b) E-plane directional diagram.
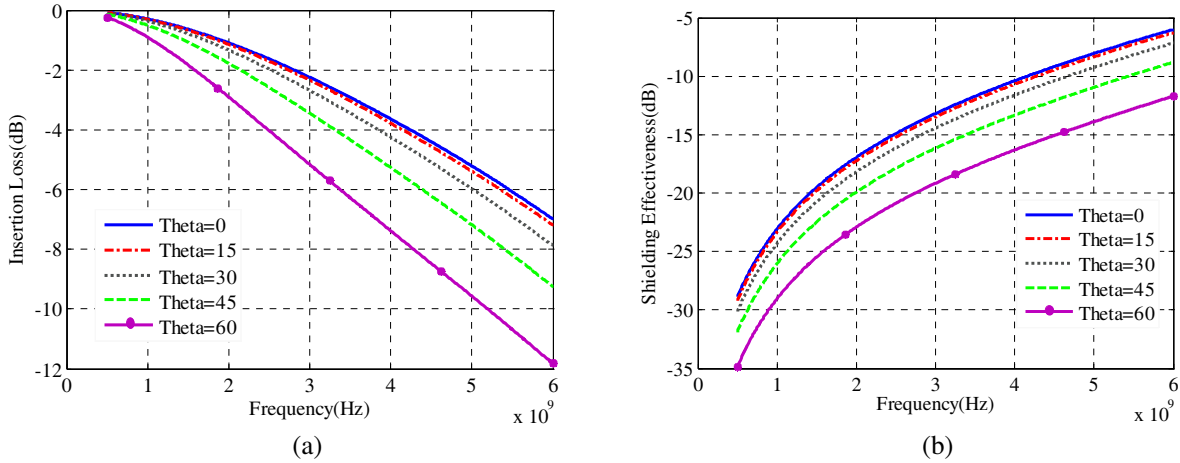
Figure 6 shows the transmission characteristic when diodes is on and off at different incident angles. When incident angle is less than 30°, transmission characteristic of ESS almost keeps stable. But as incident angle goes on increasing, shieling effectiveness and insertion loss also begin to increase rapidly.

4. EXPERIMENT RESULT AND DISCUSSION

An ESS prototype based on the improved structure was fabricated using printed circuit board technology. The ESS sample consisted of 50×50 unit cells. The substrate material was Rogers RO4350. Around the ESS unit cell, there was a metal strip with width of 10 mm at each side. The overall size of ESS prototype was about 400 mm $\times$ 400 mm. The measurement for ESS was divided into three steps. The first step was to measure insertion loss in an anechoic chamber. The second and third ones were to measure shielding effectiveness under the irradiation by HPM and UWB in outer space.

The test schematic for insertion loss was set as in Figure 7. Two ridged horns were used as transmitter antenna and receiver antenna, respectively. An absorbing wall was placed between transmitting and receiving antennas. They were put at two sides of the absorbing wall with equal distance which was about 0.7 m to insure ESS located in the far-field region. An Anritsu vector network analyzer was employed to measure the S parameters. The measured and simulated results are shown in Figure 8.

As depicted in Figure 8, insertion loss is less than 1 dB when frequency is below 1.8 GHz. The ripple in measurement results is likely caused by the diffraction at the edges of absorbing wall. Using

(a)

(b)

Figure 6. Transmission characteristic of ESS under different incident angle. (a) Insertion loss of ESS under different incident angle. (b) Shielding effectiveness of ESS under different incident angle.

Figure 7. Experiment setup for measuring insertion loss of ESS.
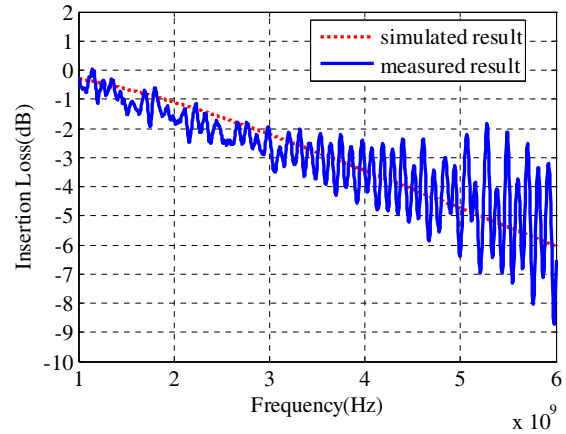
**Figure 8.** Simulation result in CST compared to measured result.

Figure 9. Measurement setup for shielding effectiveness of ESS under irradiating by HPM.

high quality absorbing material and increasing the size of absorbing wall can reduce the level of ripple.

Figure 9 shows the measurement setup for shielding effectiveness under HPM irradiation. An EMC high power source was used to produce high intensity electromagnetic wave, and a high-gain parabolic antenna was employed as receiving antenna with ESS mounted at horn aperture. A Tektronix multichannel oscilloscope put in shelter was used to record irradiation waveform. The intensity of

irradiation wave was adjusted by changing the place of parabolic antenna [19]. In experiment, the duration of irradiation was $5 \sim 10$ seconds. The pulse repetition frequency is $200\,\mathrm{Hz}$, and the pulse width is about $1\,\mathrm{\mu s}$.

The waveform recorded when ESS is not loaded at horn aperture is shown in Figure 10. Three different intensity electromagnetic waves with electric field intensities of $1500\,\mathrm{V/m}$, $1108\,\mathrm{V/m}$ and $780\,\mathrm{V/m}$ are given. Figure 11 shows the electric field passing through ESS when ESS was mounted on the aperture of horn. From Figure 11, we can see that there is a power leakage lasting less than $50\,\mathrm{ns}$ because of the switching time of PIN diodes. After PIN diode switches on, the amplitude of limiting field is about $250\,\mathrm{V/m}$ which is significantly reduced compared with the field without ESS. The size of period and the type of PIN diode are two factors influencing intensity of limiting field. The smaller the period size is, the smaller the intensity of limiting field is. To choose PIN diode with low equivalent resistance and inductance decreases the amplitude of limiting field. Another method to decrease limiting field is to add a bias voltage on diode.
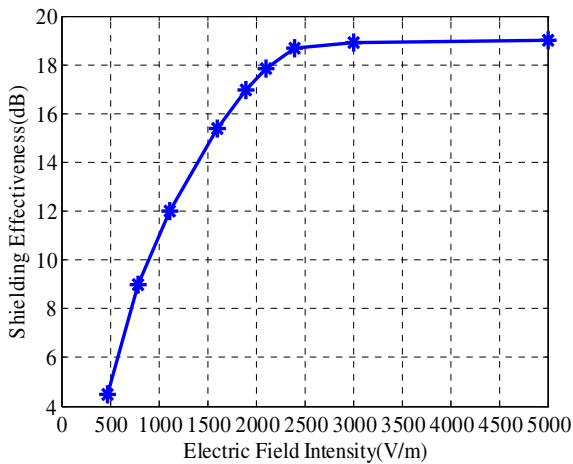
Figure 12 shows the shielding effectiveness of improved ESS under irradiating with different amplitude of electric field. When the electric field around improved ESS is low, it can pass improved ESS with low attenuation. As the intensity of radiation field increases, the shielding effectiveness also
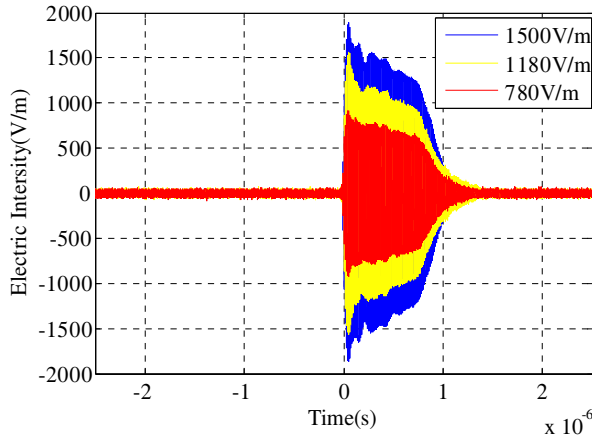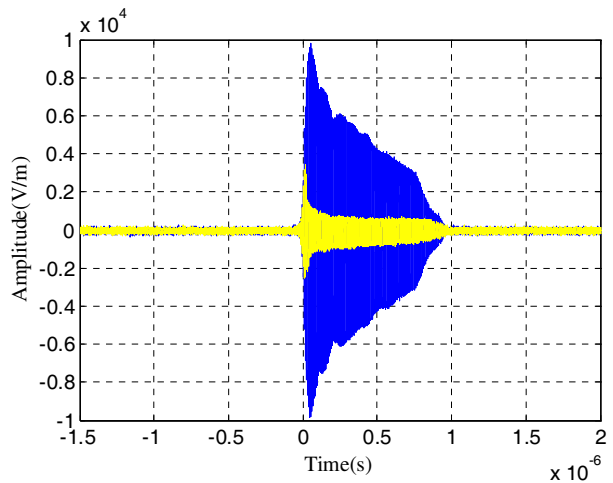

Figure 10. Free space field intensity around parabolic antenna with different transmitting amplitude.
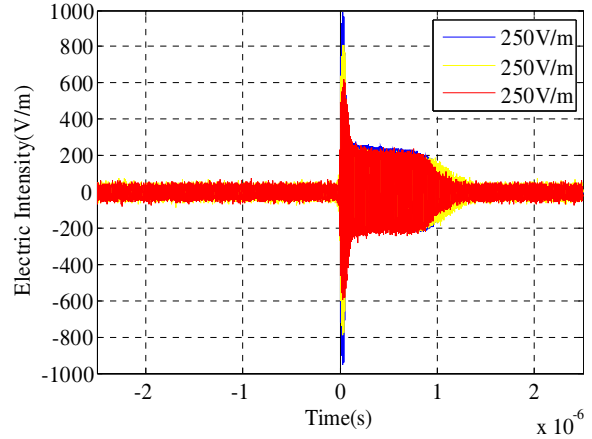
Figure 11. Electric field intensity after passing ESS with different transmitting amplitude.

Figure 12. Shielding effectiveness of ESS as a function of radiation field intensity.

Figure 13. The recorded waveform of mounted and not mounted ESS when amplitude of incident wave reaches $6000\,\mathrm{V/m}$.

increases keeping limiting field stable until it reaches about 19 dB. It is because diode reaches saturation. If the intensity of radiation field goes on increasing, the amplitude of limiting field also increases. As shown in Figure 13, when the amplitude of radiation field is about 6000 V/m, the amplitude of limiting field is about 600 V/m.

Figure 14 shows the measurement setup for shielding effectiveness under UWB irradiation. A UWB source was used to produce high power UWB irradiation electromagnetic wave. The other measurement setup was the same as measurement setup under HPM irradiation.

Figure 14. Measurement setup for shielding effectiveness of ESS under irradiating by UWB.
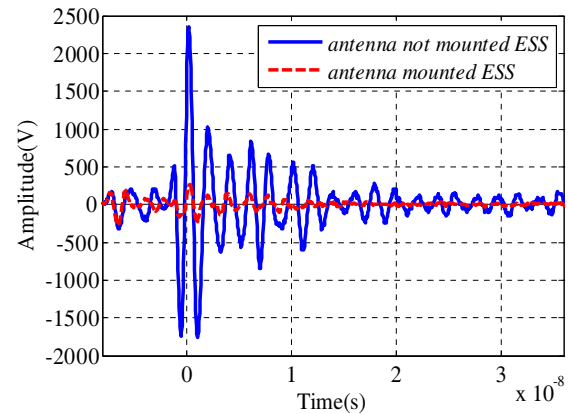
Figure 15. Comparing of electric field intensity with receiver mounted ESS or not.

As shown in Figure 15, when ESS is mounted on receiving antenna, the electric field intensity passing through ESS decreases sharply. The shielding effectiveness reaches 19.5 dB. The ripple disappears after about 10 ns which is different from the origin waveform. The reason is that diode recovering from conducting needs some time. From Figure 15, we know that ESS can be effective to defend UWB attacking with short rising time and strong intensity.

Comparing Figure 11 and Figure 15, we can find that the ESS response time irradiated by UWB is shorter than that irradiated by the HPM. The reason is that the frequency, amplitude and rising edge of the incident waves have a great influence on the response time of the ESS, where a lower frequency, higher amplitude and sharper rising edge may result in a shorter response time of ESS.

5. CONCLUSION

In this paper, an improved ESS is presented, and its systematic design method is introduced. The improved ESS decreases the insertion loss and expands working band. Through CST simulation, we find that the improved ESS has little influence on the antenna pattern. An improved ESS prototype is fabricated using printed circuit board technology. The experiment results show that the insertion loss is less than 1 dB below 1.8 GHz and that the maximum shielding effectiveness reaches 19 dB at measurement frequency under HPM irradiation, which is consistent with simulation result. UWB irradiation testing proves that the improved ESS can be applied to defend UWB attacking, and the shielding effectiveness reaches 19.5 dB.

REFERENCES

1. Sabath, F., "What can be learned from documented Intentional Electromagnetic Interference (IEMI) Attacks?" *General Assembly and Scientific Symposium*, 1–4, URSI Istanbul, 2011.

2. Sabath, F., "Classification of electromagnetic effects at system level," *International Symposium on Electromagnetic Compatibility — EMC*, 1–5, Europe, Hamburg, Germany, 2008.

3. Savage, E. and W. Radasky, *Overview of the Threat of IEMI(Intentional Electromagnetic Interference) International Symposium on Electromagnetic Compatibility (EMC)*, 312–322, Pittsburgh, USA, 2012.

4. Backstrom, M. G. and K. G. Lovstrand, "Susceptibility of electronic systems to high-power microwaves: Summary of test experience," *IEEE Transactions on Electromagnetic Compatibility*, Vol. 46, 396–403, 2004.

5. Yang, C., P. Liu, and X. Huang, "A novel method of energy selective surface for adaptive hpm/emp protection," *Antennas and Wireless Propagation Letters*, Vol. 12, 112–115, 2013.

6. Zurauskiene, N., S. Balevicius, and L. Zurauskiene, "Nanostructured manganite films as protectors against fast electromagnetic pulses," *IEEE Transactions on Plasma Science*, Vol. 41, 2890–2895, 2013.

7. Tan, J., P. Liu, C. Yang, et al., "EM simulation analysis of the Energy Selective surface," *High Voltage Engineering*, Vol. 39, 30897–30903, 2013.

8. Nilsson, T., "Investigation of limiters for HPM and UWB front-door protection," Ph.D. Dissertation, Linköping University, 2006.

9. Lee, K.-A. and K.-C. Ko, "Propagation model of high power electromagnetic pulse by using a serial-parallel resistors circuit," *IEEE Transactions on Plasma Science*, Vol. 42, 3309–3312, 2014.

10. Bolioli, S. and J. C. Joly, "Front-door protection using frequency selective surface," *International Symposium on Electromagnetic Compatibility (EMC)*, 1–4, Athens, 2009.

11. Monni, S., D. Bekers, M. van Wanum, et al., "Limiting frequency selective surface," *EuMC 2009 Microwave Conference*, 606–609, Rome European, 2009.

12. Monni, S., D. J. Bekers, M. van Wanum, et al., "Protection of RF electronics using tuneable frequency selective surfaces," *3rd European Conference on Antennas and Propagation, EuCAP 2009*, 3170–3174, Berlin, 2009.

13. Scott, S., C. D. Nordquist, M. J. Cich, et al., "A frequency selective surface with integrated limiter for receiver protection," *Antennas and Propagation Society International Symposium (APSURSI)*, 1–2, Chicago, 2012.

14. Yang, G., J. Tan, D. Sheng, et al., "Plasma limiter for Protecting against high power microwave," *Journal Of Scientific & Industrial Research*, Vol. 67, 685–687, 2008.

15. Munk, B. A., *Frequency Selective Surface: Theory and Design*, Wiley, New York, 2000.

16. Zhang, Y., M. Yuan, and Q. Liu, " Wide band response of an electromagnetic wave shield based on a diode grid," *Progress In Electromagnetic Research*, Vol. 141, 591–606, 2013.

17. Chang, K., I. K. Sang, J. Y. Young, "Equivalent circuit modeling of active frequency selective surface," *IEEE on Radio and Wireless Symposium*, 663–666, Orlando, 2008.

18. Marcuvitz, N., *Waveguide Handbook*, 280–291, McGraw-Hill, London, UK, 1951.

19. Palisek, L. and L. Suchy, "High power microwave effects on computer networks," *EMC Europe*, 18–21, York, 2011.